A bilinear partially penalized immersed finite element method for elliptic interface problems with multi-domain and triple-junction points

Yuan Chen [a], Songming Hou [b,1], Xu Zhang [c,2,*]

[a] *Department of Statistics, The George Washington University, WA, DC 20052, USA*
[b] *Program of Mathematics & Statistics and Center of Applied Physics, Louisiana Tech University, Ruston, LA 71272, USA*
[c] *Department of Mathematics, Oklahoma State University, Stillwater, OK 74078, USA*

ARTICLE INFO

ABSTRACT

In this article, we introduce a new partially penalized immersed finite element method (IFEM) for solving elliptic interface problems with multi-domain and triple-junction points. We construct new IFE functions on elements intersected with multiple interfaces or with triple-junction points to accommodate interface jump conditions. For non-homogeneous flux jump, we enrich the local approximating spaces by adding up to three local flux basis functions. Numerical experiments are carried out to show that both the Lagrange interpolations and the partial penalized IFEM solutions converge optimally in L^2 and H^1 norms.

1. Introduction

Elliptic interface problems have received wide attention in the past decades. Numerous numerical methods have been developed to generate accurate and effective approximations for interface problems. Conventional numerical methods, such as the finite element method [1], require the mesh to be aligned with the interface. Another class of numerical methods uses unfitted meshes for solving interface problems. In the finite difference framework, since the pioneering working of immersed boundary method [2], the immersed interface method [3], matched interface and boundary method [4], cut-cell method [5] have been developed. In the finite element framework, there have been penalty finite element method [6], generalized finite element method [7], extended finite element method [8], cut finite element method [9], and immersed finite element method [10], to name only a few.

The immersed finite element method (IFEM) [10–15] is a class of finite element methods that modify the approximation functions, instead of solution meshes, locally around the interface in order to resolve the interface with unfitted mesh. An IFEM adopts standard finite element basis functions on elements away from interfaces but constructs new piecewise-polynomial basis functions on elements cut through by interfaces. In [16], a partially penalized immersed finite element method (PPIFEM) was developed by adding consistency terms and penalty terms to the classical Galerkin formulation on the interface edges. The method is proved to converge optimally in the energy norm [16] and L^2 norm [17]. Moreover,

---

* Corresponding author.
E-mail addresses: yuan_chen@gwu.edu (Y. Chen), shou@latech.edu (S. Hou), xzhang@okstate.edu (X. Zhang).
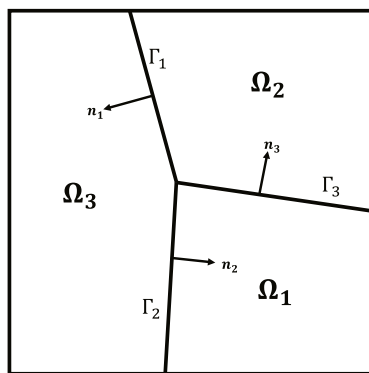
Fig. 1. A typical triple-region domain.

the PPIFEM was extended to handle non-homogeneous flux jump conditions in [18]. Gradient recovery for PPIFEM was reported in [19].

Most numerical methods aim at interface problems with two sub-domains. There are a few literatures concerning multi-domain interface problems with possibly a triple-junction point. In [20], the matched interface and boundary method has been developed on multi-domain. In [21], the authors employed a Petrov–Galerkin type method [22] to solve multi-domain interface problems. Related research papers include [23,24]. As for IFEM for multi-domain interface problems with triple junction, we developed a piecewise linear IFEM on triangular meshes [25]. One of the challenges is the construction of IFEM basis functions due to the complicated geometrical configuration of a multi-domain. We showed that the stiffness matrix is symmetric positive definite and the numerical solutions are reasonably accurate. As indicated in [16] for two-domain interface problems, we also observed that the convergence rates in L^2 and H^1 norms deteriorate as the mesh size becomes small.

In this paper, we develop a new IFEM for solving multi-domain interface problems with non-homogeneous flux jump. We use interface-unfitted rectangular Cartesian meshes, and construct the piecewise bilinear shape functions on multi-interface elements. The PPIFEM is used for enhanced accuracy and stability. Non-homogeneous flux jump conditions are handled by enriching the local approximation spaces, inspired by [26] and [18]. It is worthwhile to note that in our new construction on multi-interface elements, the number of restrictions (from nodal-value conditions and interface jump conditions) and degrees of freedom match for all types of interface elements. Therefore, the least-squares approximation is unnecessary for obtaining IFE basis functions as the piecewise-linear IFE spaces in [25]. Our numerical results indicate that the bilinear PPIFEM for multi-domain interface problems converge optimally in H^1, L^2 and L^∞ norms without deterioration even for fine meshes. Besides, the new method outperforms the classical linear IFEM [25] in the accuracy around interfaces.

The rest of this article is organized as follows. In Section 2, we introduce the multi-domain interface problems and recall some preliminary results. In Section 3, bilinear IFE basis functions and flux jump basis functions are constructed on different types of interface elements. Local and global IFE spaces are defined accordingly. In Section 4, we present the PPIFEM for multi-domain interface problems with the non-homogeneous flux jump. In Section 5, numerical examples are provided to show the features of our new method. A brief conclusion is presented in Section 6.

2. Interface problems

Let $\Omega \subset \mathbb{R}^2$ be an open bounded domain. Assume that Ω is subdivided by several interfaces into multiple domains. Without loss of generality, we assume that Ω is divided by three interfaces Γ_1, Γ_2, Γ_3 into three sub-domains Ω_1, Ω_2, Ω_3. We also assume that the boundaries $\partial\Omega_1$, $\partial\Omega_2$, $\partial\Omega_3$ are Lipschitz continuous. See Fig. 1 for an illustration of the geometric setting of the domain and interfaces.

Consider the following elliptic interface problem:

$$-\nabla \cdot (\beta \nabla u) = f, \quad \text{in } \Omega_1 \cup \Omega_2 \cup \Omega_3,$$
$$u = g, \quad \text{on } \partial\Omega. \tag{2.1}$$

The coefficient function $\beta(\mathbf{x})$ is assumed to be discontinuous across each interface Γ_i where $\mathbf{x} = (x, y)$. For simplicity, we assume that $\beta(\mathbf{x})$ is a piecewise constant function such that

$$\beta(\mathbf{x}) = \beta_i, \quad \text{if } \mathbf{x} \in \Omega_i, \tag{2.2}$$

where $\beta_i > 0$. Across each interface Γ_i, the solution u is assumed to be continuous, i.e.,

$$[\![u]\!]_{\Gamma_i} = 0, \quad \forall i = 1, 2, 3. \tag{2.3}$$

The normal flux jumps are prescribed as follows:

$$\begin{cases} [\![\beta \nabla u \cdot \mathbf{n}]\!]_{\Gamma_1} \triangleq (\beta_3 \nabla u_3 - \beta_2 \nabla u_2) \cdot \mathbf{n}_1 = b_1(x, y) & \text{on } \Gamma_1, \\ [\![\beta \nabla u \cdot \mathbf{n}]\!]_{\Gamma_2} \triangleq (\beta_1 \nabla u_1 - \beta_3 \nabla u_3) \cdot \mathbf{n}_2 = b_2(x, y) & \text{on } \Gamma_2, \\ [\![\beta \nabla u \cdot \mathbf{n}]\!]_{\Gamma_3} \triangleq (\beta_2 \nabla u_2 - \beta_1 \nabla u_1) \cdot \mathbf{n}_3 = b_3(x, y) & \text{on } \Gamma_3. \end{cases} \tag{2.4}$$

Here, $u_i = u|_{\Omega_i}$, and b_i, $i = 1, 2, 3$, are given functions defined on Γ_i. Unit normal vectors of $\Gamma_1, \Gamma_2, \Gamma_3$ are denoted by $\mathbf{n}_1$, $\mathbf{n}_2$, $\mathbf{n}_3$, respectively. For simplicity, we also use $g_i = g|_{\partial\Omega_i \cap \partial\Omega}$ from now on.

We use the standard notations for the Sobolev spaces. Define the broken Sobolev space

$$\tilde{H}^2(\Omega) = \left\{ v \in H^1(\Omega) : v|_{\Omega_i} \in H^2(\Omega_i), \ \ [\![\beta \nabla u \cdot \mathbf{n}]\!]_{\Gamma_i} = b_i, \ i = 1, 2, 3 \right\},$$

equipped with the semi-norm and norm:

$$|u|_{\tilde{H}^2(\Omega)} = \left(\sum_{i=1}^3 |u|_{H^2(\Omega_i)}^2 \right)^{1/2}, \quad \|u\|_{\tilde{H}^2(\Omega)} = \left(\|u\|_{H^1(\Omega)}^2 + |u|_{\tilde{H}^2(\Omega)}^2 \right)^{1/2}.$$

The variational form of (2.1)–(2.4) is to find $u \in H^1(\Omega)$ such that $u = g$ on $\partial\Omega$ and

$$a(u, v) := (\beta \nabla u, \nabla v) = (f, v) - \sum_{i=1}^3 (b_i, v)_{\Gamma_i}, \quad \forall v \in H_0^1(\Omega), \tag{2.5}$$

where $(\cdot, \cdot)_\omega$ is the L^2 inner product on $\omega \subseteq \Omega$. The subscript ω is omitted when $\omega = \Omega$.

For elliptic interface problems, the following regularity result holds [27]:

Theorem 2.1. *Assume that $f \in L^2(\Omega)$, $g \in H^{3/2}(\partial\Omega_i \cap \partial\Omega)$, for $i = 1, 2, 3$. Then the problem* (2.1)–(2.4) *has a unique solution $u \in H^1(\Omega)$ such that for some constant $C > 0$,*

$$\|u\|_{\tilde{H}^2(\Omega)} \le C \left(\|f\|_{L^2(\Omega)} + \sum_{i=1}^3 \|b_i\|_{H^{1/2}(\Gamma_i)} + \sum_{i=1}^3 \|g_i\|_{H^{3/2}(\partial\Omega_i \cap \partial\Omega)} \right). \tag{2.6}$$

3. Construction of triple-junction bilinear IFE spaces

In this section, we construct the bilinear IFE space on interface elements with multiple interfaces. The construction of classical bilinear IFE functions with one interface is reported in [28,29].

3.1. Element classification

Let $\mathcal{T}_h$ be an interface-independent Cartesian mesh of Ω where h denotes the mesh size. We classify all rectangular elements according to the number of interfaces intersecting the interior of an element. If the interior of an element $T \in \mathcal{T}_h$ is not intersected with any interface Γ_i, then the element T is called a non-interface (or a regular) element. The collection of all regular elements are denoted by $\mathcal{T}_h^n$. If the interior of an element $T \in \mathcal{T}_h$ is cut through by at least one interface Γ_i, then the element T is called an interface element. The collection of these elements is denoted by $\mathcal{T}_h^i$. For multi-interface problems, we assume that the interface elements satisfy the following hypotheses:

(H1) Multiple interfaces can only intersect with an element at no more than three edges.

(H2) Each edge of an interface element can only intersect with interfaces at no more than two points unless the edge is part of the interface.

These hypotheses rule out the case that interfaces intersect an element at three points but on the same edge. Furthermore, we distinguish the collection of interface elements $\mathcal{T}_h^i$ by three sub-categories based on the number of interfaces inside an element. For a triple-domain interface problem stated above, there are at most three interfaces inside an element. The set $\mathcal{T}_{h,1}^i$ contains elements intersected with only one interface. The set $\mathcal{T}_{h,2}^i$ includes all elements intersecting two interfaces (see Fig. 3 for an illustration). The set $\mathcal{T}_{h,3}^i$ contains the elements intersecting with all three interfaces and hence the triple-junction points must be inside these elements (see Fig. 4 for an illustration).

Now all elements in a Cartesian mesh must be in one of the following classes.

$$\mathcal{T}_h = \mathcal{T}_h^n \cup \mathcal{T}_h^i = \mathcal{T}_h^n \cup \mathcal{T}_{h,1}^i \cup \mathcal{T}_{h,2}^i \cup \mathcal{T}_{h,3}^i. \tag{3.1}$$

Fig. 2 illustrates the above classification of elements by color. Elements in white denote regular elements. Elements in green denote the case when an interface touches one of the nodes of the element or overlaps with an edge of the element. Elements in both of these two colors represent elements in $\mathcal{T}_h^n$. Elements marked in red, orange, and blue represent elements in $\mathcal{T}_{h,1}^i$, $\mathcal{T}_{h,2}^i$, and $\mathcal{T}_{h,3}^i$, respectively.
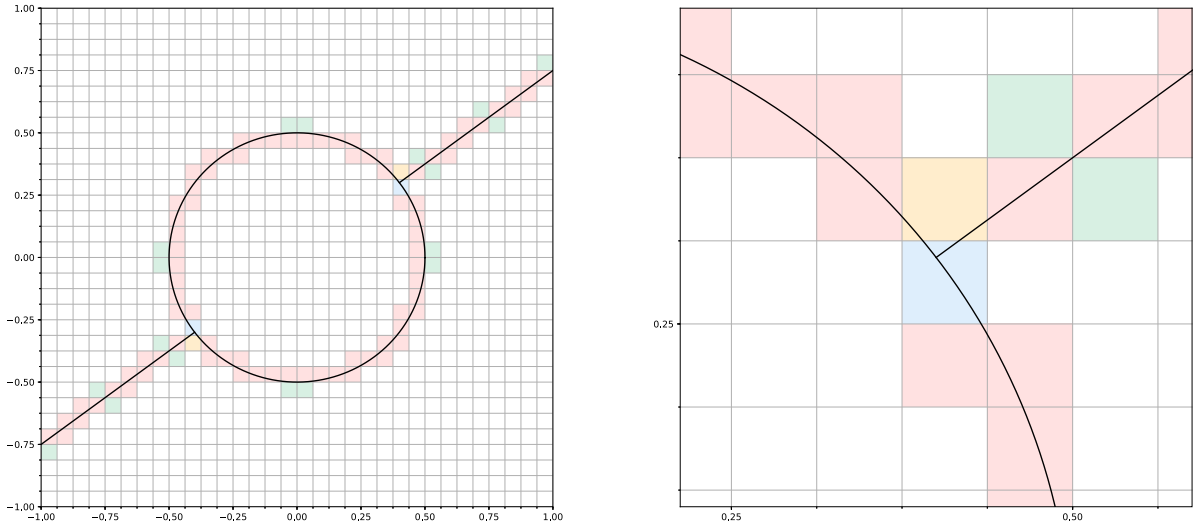
Fig. 2. Left: a typical triple-region domain and a Cartesian mesh. Right: a zoom-in of the region around triple point.
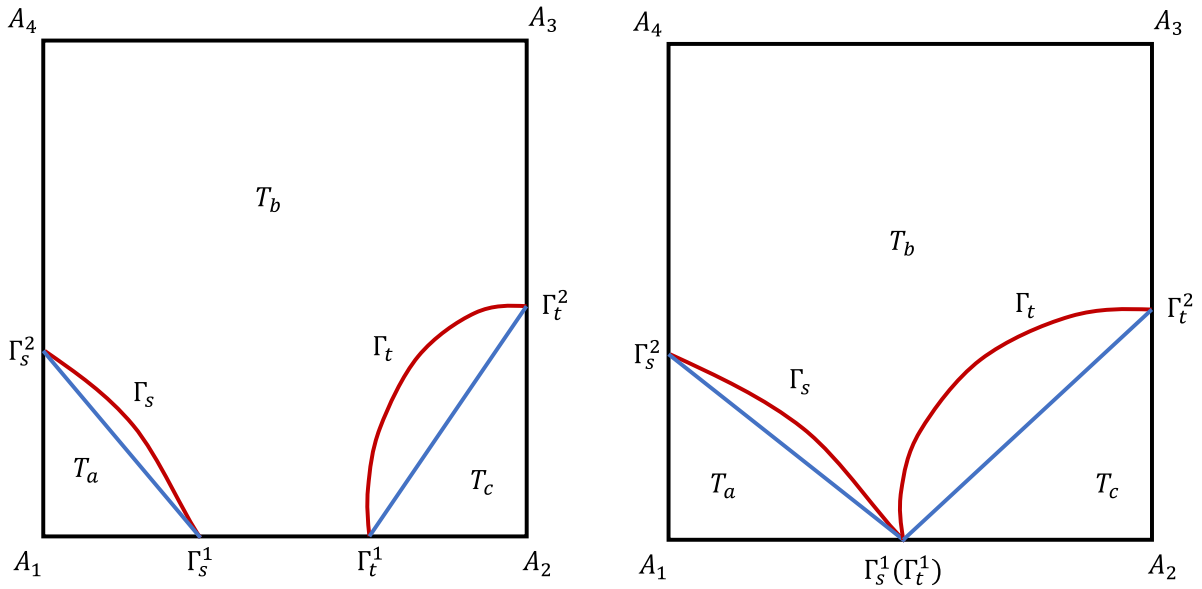
Fig. 3. Two typical elements in $\mathcal{T}_{h,2}^i$.

Remark 3.1. If the triple-junction point is on an edge of an element (see the right plot of Fig. 3), we count this element in $\mathcal{T}_{h,2}^i$.

3.2. Local IFE spaces on $T \in \mathcal{T}_h^n$ and $T \in \mathcal{T}_{h,1}^i$

On a non-interface element $T \in \mathcal{T}_h^n$, we adopt the standard bilinear ($\mathbb{Q}_1$) nodal basis functions. The local finite element space on T is

$$S_h(T) = \mathrm{span}\{1, x, y, xy\}.$$

If an element $T \in \mathcal{T}_{h,1}^i$, then T intersects with only one interface at two different points at two edges. We refer the readers to the construction of the classical bilinear IFE basis functions in [28,29]. For the non-homogeneous flux jump, the local space is enlarged by adding one more basis function that vanishes at all nodes, continuous over the element, but with a unit flux jump. For more details, we refer readers to [26]. Our main focus is to construct the local approximating spaces on elements in $\mathcal{T}_{h,2}^i$ and $\mathcal{T}_{h,3}^i$.

Fig. 4. Two typical elements in $\mathcal{T}_{h,3}^i$.

3.3. Local IFE spaces on $T \in \mathcal{T}_{h,2}^i$

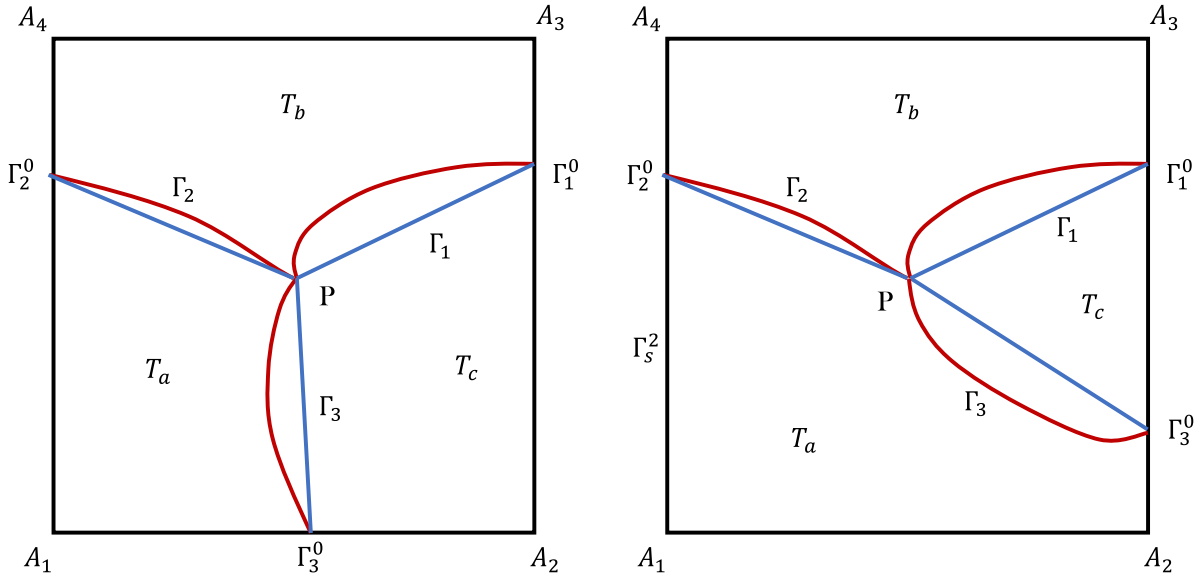In this case, there are two interfaces inside an element $T \in \mathcal{T}_{h,2}^i$. As shown in Fig. 3, the triple-junction point is disjoint of the interior of the element (left plot of Fig. 3) or lie on the edge of the element (right plot of Fig. 3). Let the curved interfaces be approximated by the line segments Γ_s, Γ_t, and they split the element T into three polygons, denoted by T_a, T_b, T_c. The intersection points are denoted by Γ_s^1, Γ_s^2, Γ_t^1, and Γ_t^2. See Fig. 3 for the geometrical configuration.

We define four piecewise bilinear basis functions on an element as follows

$$\phi_{i,T}(\mathbf{x}) = \begin{cases} \phi_{i,T}^a(\mathbf{x}) = a_1 + b_1 x + c_1 y + d_1 xy, & \text{if } \mathbf{x} \in T_a, \\ \phi_{i,T}^b(\mathbf{x}) = a_2 + b_2 x + c_2 y + d_2 xy, & \text{if } \mathbf{x} \in T_b, \qquad i = 1, 2, 3, 4. \\ \phi_{i,T}^c(\mathbf{x}) = a_3 + b_3 x + c_3 y + d_3 xy, & \text{if } \mathbf{x} \in T_c, \end{cases} \tag{3.2}$$

The following nodal-value conditions and the interface jump conditions are used to determine the coefficients a_j, b_j, c_j, and d_j, $(j = 1, 2, 3)$:

- four nodal-value conditions

$$\phi_{i,T}(A_j) = \delta_{ij}, \quad \forall i, j = 1, 2, 3, 4. \tag{3.3}$$

- six continuity conditions of the basis functions

$$\begin{aligned} \phi_{i,T}^a(\Gamma_s^1) = \phi_{i,T}^b(\Gamma_s^1), & \quad \phi_{i,T}^a(\Gamma_s^2) = \phi_{i,T}^b(\Gamma_s^2), & d_1 = d_2, \\ \phi_{i,T}^b(\Gamma_t^1) = \phi_{i,T}^c(\Gamma_t^1), & \quad \phi_{i,T}^b(\Gamma_t^2) = \phi_{i,T}^c(\Gamma_t^2), & d_2 = d_3. \end{aligned} \tag{3.4}$$

- two conditions of normal flux continuity

$$\int_{\Gamma_s \cap T} \left[\!\left[\beta \nabla \phi_{i,T} \cdot \mathbf{n} \right]\!\right]_{\Gamma_s} ds = 0, \qquad \int_{\Gamma_t \cap T} \left[\!\left[\beta \nabla \phi_{i,T} \cdot \mathbf{n} \right]\!\right]_{\Gamma_t} ds = 0. \tag{3.5}$$

The twelve conditions in (3.3)–(3.5) are used to determine the twelve coefficients a_i, b_i, c_i, and d_i, with $i = 1, 2, 3$ in a bilinear IFE local basis function $\phi_{i,T}$, $i = 1, 2, 3, 4$. The left plot of Fig. 5 exemplifies a typical bilinear IFE basis function on $T \in \mathcal{T}_{h,2}^i$. The local bilinear IFE space is defined as $S_h(T) = \text{span}\{\phi_{i,T} : i = 1, 2, 3, 4\}$.

To accommodate the non-homogeneous jump of flux (2.4), we enrich the local IFE space by adding two local functions $\phi_{T,J}^k$, $k = 1, 2$. These flux basis functions are also defined as piecewise bilinear polynomials

$$\phi_{T,J}^k(\mathbf{x}) = \begin{cases} \phi_{T,J}^{k,a}(\mathbf{x}) = a_1 + b_1 x + c_1 y + d_1 xy, & \text{if } \mathbf{x} \in T_a, \\ \phi_{T,J}^{k,b}(\mathbf{x}) = a_2 + b_2 x + c_2 y + d_2 xy, & \text{if } \mathbf{x} \in T_b, \qquad k = s, t. \\ \phi_{T,J}^{k,c}(\mathbf{x}) = a_3 + b_3 x + c_3 y + d_3 xy, & \text{if } \mathbf{x} \in T_c, \end{cases} \tag{3.6}$$
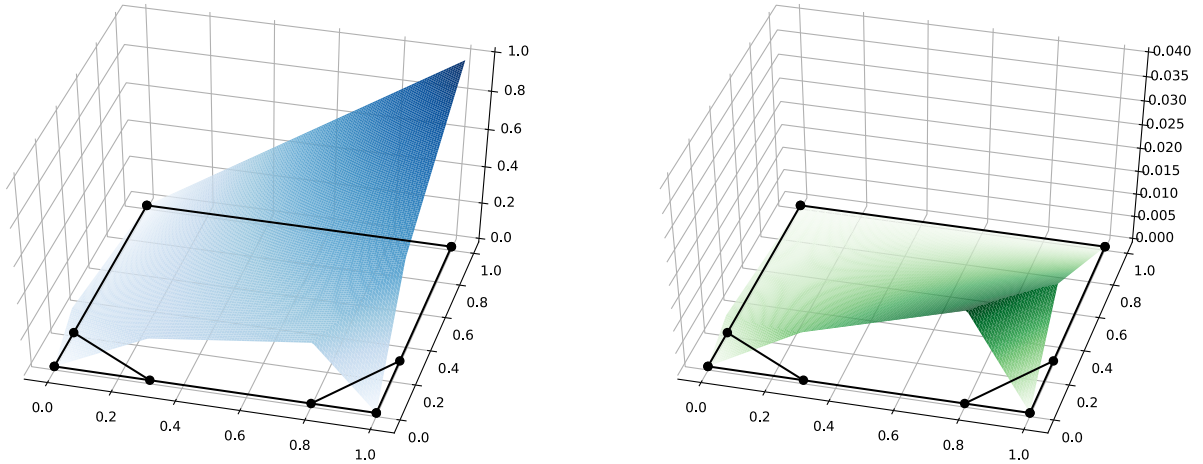
Fig. 5. Basis function(left) and flux jump function(right) of elements in $\mathcal{T}_{h,2}^i$.

The flux jump basis functions $\phi_{T,J}^s$ and $\phi_{T,J}^t$ satisfy the following conditions

- They vanish at four nodes A_j of the element T:

$$\phi_{T,J}^k(A_j) = 0, \quad \forall j = 1, 2, 3, 4, \quad k = s, t. \tag{3.7}$$

- They are continuous across the endpoints of interfaces $\Gamma_i \cap T$:

$$\begin{aligned}
\phi_{T,J}^{k,a}(\Gamma_s^1) &= \phi_{T,J}^{k,b}(\Gamma_s^1), \quad \phi_{T,J}^{k,a}(\Gamma_s^2) = \phi_{T,J}^{k,b}(\Gamma_s^2), \quad d_1 = d_2, \\
\phi_{T,J}^{k,a}(\Gamma_t^1) &= \phi_{T,J}^{k,b}(\Gamma_t^1), \quad \phi_{T,J}^{k,a}(\Gamma_t^2) = \phi_{T,J}^{k,b}(\Gamma_t^2), \quad d_2 = d_3.
\end{aligned} \tag{3.8}$$

- They have a unit flux jump on the corresponding interfaces.

$$\int_{\Gamma_{k'} \cap T} \left[\!\left[\beta \nabla \phi_{T,J}^k \cdot \mathbf{n} \right]\!\right]_{\Gamma_{k'}} ds = \delta_{kk'}, \quad \forall k' = s, t. \tag{3.9}$$

A flux basis function of this type is shown in the right plot of Fig. 5. The local flux IFE space $S_h^J(T) = \mathrm{span}\{\phi_{T,J}^s, \phi_{T,J}^t\}$ and the enriched local IFE space on T is $\tilde{S}_h(T) = S_h(T) \cup S_h^J(T)$. The Lagrange type interpolation $\mathcal{I}_{h,T} : \tilde{H}^2(T) \to \tilde{S}_h(T)$ is as follows

$$\mathcal{I}_{h,T} u(\mathbf{x}) = \sum_{i=1}^{3} u(A_i) \phi_{i,T}(\mathbf{x}) + \sum_{k=s,t} q_T^k \phi_{T,J}^k(\mathbf{x}), \tag{3.10}$$

where

$$q_T^k = \int_{\Gamma_k \cap T} \left[\!\left[\beta \nabla u \cdot \mathbf{n} \right]\!\right]_{\Gamma_k} ds. \tag{3.11}$$

3.4. Local IFE spaces on $T \in \mathcal{T}_{h,3}^i$

In this case, an element $T \in \mathcal{T}_{h,3}^i$ intersects all three interfaces at three points. In general, the triple-junction point, denoted by P, is inside this element. See Fig. 4 for an illustration.

We use the line approximations of the curved interfaces by Γ_1, Γ_2, Γ_3, which split the whole rectangle into three polygons, denoted by T_a, T_b, T_c (see Fig. 4). The intersection points with each interface Γ_1, Γ_2, Γ_3 are denoted by Γ_1^0, Γ_2^0, and Γ_3^0, respectively.

Piecewise bilinear IFE basis functions are constructed on the element T as follows

$$\phi_{i,T}(\mathbf{x}) = \begin{cases} \phi_{i,T}^a(\mathbf{x}) = a_1 + b_1 x + c_1 y + d_1 xy, & \text{if } \mathbf{x} \in T_a, \\ \phi_{i,T}^b(\mathbf{x}) = a_2 + b_2 x + c_2 y + d_2 xy, & \text{if } \mathbf{x} \in T_b, \quad i = 1, 2, 3, 4. \\ \phi_{i,T}^c(\mathbf{x}) = a_3 + b_3 x + c_3 y + d_3 xy, & \text{if } \mathbf{x} \in T_c. \end{cases} \tag{3.12}$$
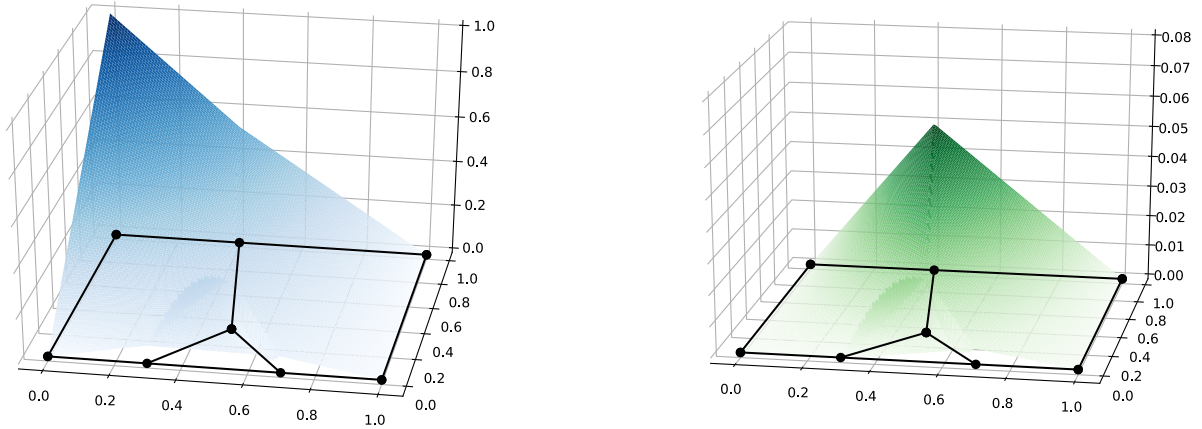
Fig. 6. A bilinear IFE local basis function(left) and a flux basis function (right) of elements in $\mathcal{T}_{h,3}^i$.

As before, the twelve coefficients are determined by

- four-nodal value conditions

$$\phi_{i,T}(A_j) = \delta_{ij}, \quad \forall i,j = 1,2,3,4. \tag{3.13}$$

- five continuity conditions of the basis functions

$$\phi_{i,T}^b(\Gamma_1^0) = \phi_{i,T}^c(\Gamma_1^0), \quad \phi_{i,T}^a(\Gamma_2^0) = \phi_{i,T}^b(\Gamma_2^0), \quad \phi_{i,T}^a(\Gamma_3^0) = \phi_{i,T}^c(\Gamma_3^0),$$
$$\phi_{i,T}^a(P) = \phi_{i,T}^b(P), \quad \phi_{i,T}^b(P) = \phi_{i,T}^c(P). \tag{3.14}$$

- three conditions of normal flux continuity

$$\int_{\Gamma_k \cap T} [\beta \nabla \phi_{i,T} \cdot \mathbf{n}]_{\Gamma_k} ds = 0, \quad k = 1,2,3. \tag{3.15}$$

A typical bilinear IFE basis function is plotted in the left plot of Fig. 6. The local bilinear IFE space is defined as $S_h(T) = \text{span}\{\phi_{i,T} : i = 1,2,3,4\}$.

For non-homogeneous jump of flux (2.4), we enrich the local IFE space by adding three local functions $\phi_{T,J}^k$, $k = 1,2,3$ as follows

$$\phi_{T,J}^k(\mathbf{x}) = \begin{cases} \phi_{T,J}^{k,a}(\mathbf{x}) = a_1 + b_1 x + c_1 y + d_1 xy, & \text{if } \mathbf{x} \in T_a, \\ \phi_{T,J}^{k,b}(\mathbf{x}) = a_2 + b_2 x + c_2 y + d_2 xy, & \text{if } \mathbf{x} \in T_b, \quad k = 1,2,3, \\ \phi_{T,J}^{k,c}(\mathbf{x}) = a_3 + b_3 x + c_3 y + d_3 xy, & \text{if } \mathbf{x} \in T_c. \end{cases} \tag{3.16}$$

such that for $k = 1,2,3$ the following conditions hold

- vanishing at four nodes A_j of the element T:

$$\phi_{T,J}^k(A_j) = 0, \quad \forall j = 1,2,3,4. \tag{3.17}$$

- continuous across the endpoints of interfaces $\Gamma_i \cap T$:

$$\phi_{T,J}^{k,b}(\Gamma_1^0) = \phi_{T,J}^{k,c}(\Gamma_1^0), \quad \phi_{T,J}^{k,a}(\Gamma_2^0) = \phi_{T,J}^{k,b}(\Gamma_2^0), \quad \phi_{T,J}^{k,a}(\Gamma_3^0) = \phi_{T,J}^{k,c}(\Gamma_3^0),$$
$$\phi_{T,J}^{k,a}(P) = \phi_{T,J}^{k,b}(P), \quad \phi_{T,J}^{k,b}(P) = \phi_{T,J}^{k,c}(P). \tag{3.18}$$

- unit flux jump condition:

$$\int_{\Gamma_j \cap T} [\beta \nabla \phi_{T,J}^k \cdot \mathbf{n}]_{\Gamma_j} ds = \delta_{kj}, \quad \forall j = 1,2,3. \tag{3.19}$$

A flux basis function of this type is shown in the right plot of Fig. 6. The local flux space is defined by $S_h^J(T) = \text{span}\{\phi_{T,J}^1, \phi_{T,J}^2, \phi_{T,J}^3\}$. As before, the enriched local IFE space on T is $\tilde{S}_h(T) = S_h(T) \cup S_h^J(T)$. The Lagrange type interpolation

$\mathcal{I}_{h,T} : \tilde{H}^2(T) \to \tilde{S}_h(T)$ is as follows

$$\mathcal{I}_{h,T}u(\mathbf{x}) = \sum_{i=1}^{4} u(A_i)\phi_{i,T}(\mathbf{x}) + \sum_{k=1}^{3} q_T^k \phi_{T,J}^k(\mathbf{x}), \tag{3.20}$$

where arguments q_T^k, $k = 1, 2, 3$, are integrations of flux jump along the interface, i.e.,

$$q_T^k = \int_{\Gamma_k \cap T} [\beta \nabla u \cdot \mathbf{n}]_{\Gamma_k} ds. \tag{3.21}$$

Remark 3.2. On an element $T \in \mathcal{T}_{h,2}^i$, the bilinear IFE basis functions degenerate to standard bilinear IFE basis functions in [29] when an interface moves out of the element. This can be proved following the same idea in [15].

Remark 3.3. Comparing with the linear IFE basis functions on the triple-junction element in [25], the bilinear IFE basis functions and flux basis functions on the rectangular element ensure the nodal-value conditions precisely. Inside the triple-junction element, the continuity is guaranteed at the intersection points and triple junction point.

3.5. Global bilinear IFE space

Now we define the global bilinear IFE space and flux IFE space. Let $\mathcal{N}_h$ be the collection of all interior nodes of the mesh $\mathcal{T}_h$. Associated with each node $\mathbf{x}_i \in \mathcal{N}_h$, we define a global bilinear IFE function Φ_i such that

(i) $\Phi_i(x_j) = \delta_{ij}$, $\forall i, j \in \mathcal{N}_h$.

(ii) $\Phi_i|_T \in S_h(T)$, $\forall T \in \mathcal{T}_h$,

where $S_h(T)$ is the local IFE space defined in previous subsections. Correspondingly, the global bilinear IFE space is defined as

$$S_h(\Omega) = \text{span}\{\Phi_i : i = 1, 2, \ldots, |\mathcal{N}_h|\}.$$

For each local flux basis $\phi_{T,J}^k$, a zero-extension to the whole domain will yield the corresponding global flux basis function $\Phi_{T,J}^k$:

$$\Phi_{T,J}^k(\mathbf{x}) = \begin{cases} \phi_{T,J}^k(\mathbf{x}), & \text{if } \mathbf{x} \in T, \\ 0, & \text{if } \mathbf{x} \notin T. \end{cases} \tag{3.22}$$

Here, the value k depends on the type of interface element. In particular, $k = 1$ if $T \in \mathcal{T}_{h,1}^i$, $k = 1, 2$ if $T \in \mathcal{T}_{h,2}^i$, and $k = 1, 2, 3$ if $T \in \mathcal{T}_{h,3}^i$. The flux jump IFE space is defined as

$$S_h^J(\Omega) = \text{span}\{\Phi_{T,J}^k : \forall T \in \mathcal{T}_h^i\},$$

and the enriched global bilinear IFE space is $\tilde{S}_h(\Omega) = S_h(\Omega) \cup S_h^J(\Omega)$.

The Lagrange interpolation operator $\mathcal{I}_h : \tilde{H}^2(\Omega) \to \tilde{S}_h$ is

$$\mathcal{I}_h u(\mathbf{x}) = \sum_{j \in \mathcal{N}_h} u(\mathbf{x}_j)\Phi_j(\mathbf{x}) + \sum_{T \in \mathcal{T}_h^i} \sum_{k=1}^{d_k} q_T^k \Phi_{T,J}^k(\mathbf{x}), \tag{3.23}$$

where $d_k = 1$ for $T \in \mathcal{T}_{h,2}^i$, $d_k = 2$ for $T \in \mathcal{T}_{h,2}^i$, and $d_k = 3$ for $T \in \mathcal{T}_{h,3}^i$. The value of q_T^k is given in (3.11) and (3.21).

4. PPIFEM For triple-junction interface problems

Let $\mathcal{E}_h$ be the collection of edges on the mesh $\mathcal{T}_h$. Let $\mathring{\mathcal{E}}_h$ and $\mathcal{E}_h^b$ be the set interior edges and boundary edges, respectively. If an edge $e \in \mathcal{E}_h$ intersects with the interface, we call it an interface edge, otherwise, it is called a non-interface edge. Denote by $\mathcal{E}_h^i$ and $\mathcal{E}_h^n$ the set of interface edges and non-interface edges, respectively.

For any interior edge $e \in \mathring{\mathcal{E}}_h$, we denote the two elements sharing the edge e by $T_{e,1}$ and $T_{e,2}$. For a function u defined on $T_{e,1} \cup T_{e,2}$, we define the average and jump of u across the edge e respectively by

$$\{\{u\}\}_e = \frac{1}{2}((u|_{T_{e,1}})|_e + (u|_{T_{e,2}})_e), \quad [\![u]\!]_e = (u|_{T_{e,1}})|_e - (u|_{T_{e,2}})_e.$$

For $e \in \mathcal{E}_h^b$, we define $\{\{u\}\}_e = [\![u]\!]_e = u|_e$.

The bilinear IFE approximation is to find $\tilde{u}_h \in \tilde{S}_h(\Omega)$ in the following form

$$\tilde{u}_h = u_h + u_h^J \triangleq \sum_{j \in \mathcal{N}_h} u_j \Phi_j + \sum_{T \in \mathcal{T}_h^i} \sum_{k=1}^{3} q_T^k \Phi_{T,J}^k, \tag{4.1}$$

where $u_h \in S_h$ is the unknown function, and $u_h^J \in S_h^J$ can be explicitly constructed. We use the PPIFEM [16] for solving the nonhomogeneous flux triple-junction interface problem: Find $u_h \in S_h$ such that

$$a_h(u_h, v_h) = (f, v_h) - a_h(u_h^J, v_h) + \sum_{i=1}^{3} (b_i, v_h)_{\Gamma_i}, \quad \forall v_h \in S_h, \tag{4.2}$$

where the bilinear form

$$\begin{aligned}
a_h(u_h, v_h) = \sum_{K \in \mathcal{T}_h} \int_K \beta \nabla v_h \cdot \nabla u_h d\mathbf{x} - \sum_{e \in \mathcal{E}_h^i} \int_e \{\!\{\beta \nabla u_h \cdot \mathbf{n}_e\}\!\} [\![v_h]\!] \, ds \\
+ \epsilon \sum_{e \in \mathcal{E}_h^i} \int_e \{\!\{\beta \nabla v_h \cdot \mathbf{n}_e\}\!\} [\![u_h]\!] \, ds + \sum_{e \in \mathcal{E}_h^i} \int_e \frac{\sigma_e}{|e|} [\![v_h]\!] [\![u_h]\!] \, ds.
\end{aligned} \tag{4.3}$$

Here, ϵ has the following choices. When $\epsilon = -1$, the scheme is called symmetric PPIFEM. When $\epsilon = 0, 1$, the scheme is called incomplete PPIFEM and non-symmetric PPIFEM, respectively. The stability parameter $\sigma_e > 0$.

5. Numerical examples

In this section, we test our new bilinear IFE approximation in two numerical examples. The numerical experiments are carried out on a group of Cartesian meshes with $N \times N$ rectangular elements, starting from $N = 16$. We consider the following three norms of the numerical solution:

$$\|u_h - u\|_{L^\infty} = \max_{(x,y) \in \mathcal{N}_h} |u_h(x, y) - u(x, y)|,$$

$$\|u_h - u\|_{L^2} = \int_\Omega |u_h(x, y) - u(x, y)|^2 dxdy,$$

$$|u_h - u|_{H^1} = \int_\Omega |\nabla u_h(x, y) - \nabla u(x, y)|^2 dxdy,$$

where $\mathcal{N}_h$ denotes the set of all nodes in the mesh $\mathcal{T}_h$. To avoid redundance, we only report errors of symmetric PPIFEM, since the results from the nonsymmetric and incomplete PPIFEM are similar.

5.1. Example 1 (straight-line interface)

In this example, we consider a square domain $\Omega = (-1, 1)^2$ separated by three straight-line interfaces. The interfaces are defined through the following level set functions:

$$\varphi_1(x, y) = \frac{38}{7}x + y - \frac{9}{28},$$
$$\varphi_2(x, y) = 5.25x + y - 0.3125,$$
$$\varphi_3(x, y) = \frac{1}{19}x + y - \frac{1}{19}.$$

The exact solution of this problem is set to be

$$u_1(x, y) = \frac{1}{\beta_1} \sin[(\frac{1}{19}x + y - \frac{1}{19})(5.25x + y - 0.3125)],$$
$$u_2(x, y) = \frac{1}{\beta_2} \sin[(\frac{1}{19}x + y - \frac{1}{19})(\frac{38}{7}x + y - \frac{9}{28})],$$
$$u_3(x, y) = \frac{1}{\beta_3} \sin[(\frac{38}{7}x + y - \frac{9}{28})(5.25x + y - 0.3125)/10].$$

The geometry of the interface and the element classifications are displayed in the left plot of Fig. 7.

We first consider the case with a moderate jump $(\beta_1, \beta_2, \beta_3) = (10, 1, 100)$. Interpolation errors in L^2, and semi-H^1 norms are reported in Table 1. The errors and convergence rates of the PPIFEM solutions are reported in Table 2. It can be observed that both the interpolations and PPIFEM solutions converge with optimal rates in all three norms. For
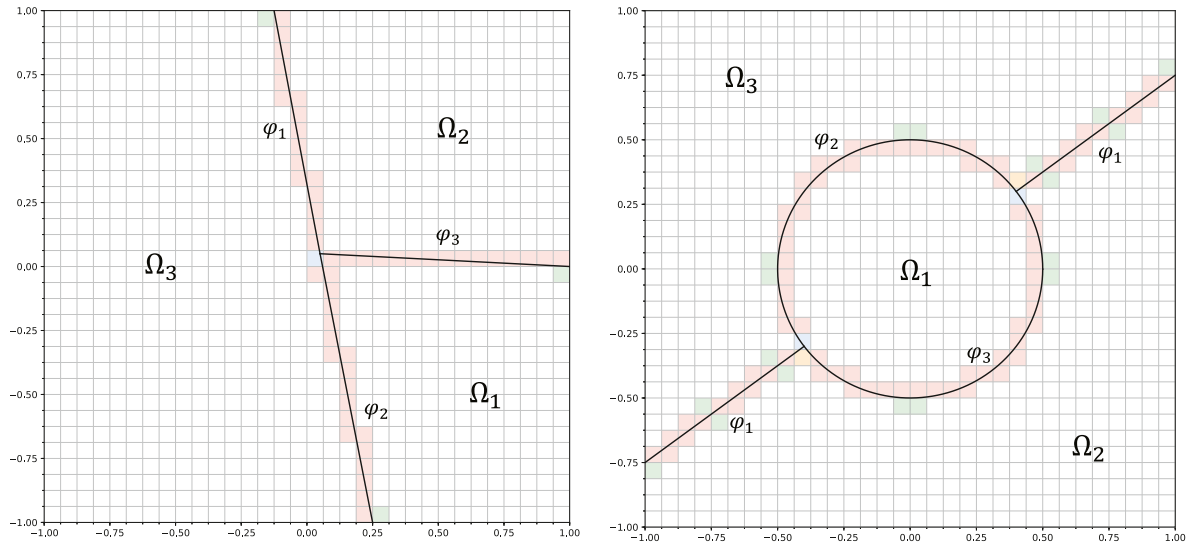
Fig. 7. Geometry of the interface and element classification for Example 1 (left) and Example 2 (right).

Table 1
Interpolation errors and convergences of Example 1 with coefficients (10,1,100).

N	$\|\mathcal{I}_h u - u\|_{L^2}$	Order	$\|\mathcal{I}_h u - u\|_{H^1}$	Order
16	3.05×10^{-2}		6.05×10^{-1}	
32	7.71×10^{-3}	1.98	3.02×10^{-1}	1.00
64	1.93×10^{-3}	2.00	1.51×10^{-1}	1.00
128	4.84×10^{-4}	2.00	7.52×10^{-2}	1.00
256	1.21×10^{-4}	2.00	3.76×10^{-2}	1.00
512	3.02×10^{-5}	2.00	1.88×10^{-2}	1.00

Table 2
PPIFEM errors in Example 1 with coefficients (10,1,100).

N	$\|u_h - u\|_{L^\infty}$	Order	$\|u_h - u\|_{L^2}$	Order	$\|u_h - u\|_{H^1}$	Order
16	2.70×10^{-2}		2.81×10^{-2}		6.05×10^{-1}	
32	6.92×10^{-3}	1.96	7.10×10^{-3}	1.98	3.02×10^{-1}	1.00
64	1.75×10^{-3}	1.99	1.78×10^{-3}	2.00	1.51×10^{-1}	1.00
128	4.38×10^{-4}	2.00	4.45×10^{-4}	2.00	7.52×10^{-2}	1.00
256	1.09×10^{-4}	2.00	1.11×10^{-4}	2.00	3.76×10^{-2}	1.00
512	2.74×10^{-5}	2.00	2.78×10^{-5}	2.00	1.88×10^{-2}	1.00

Table 3
IFEM errors in Example 1 with coefficients (10,1,100).

N	$\|u_h - u\|_{L^\infty}$	Order	$\|u_h - u\|_{L^2}$	Order	$\|u_h - u\|_{H^1}$	Order
16	2.79×10^{-2}		2.83×10^{-2}		6.08×10^{-1}	
32	8.28×10^{-3}	1.75	7.16×10^{-3}	1.98	3.04×10^{-1}	1.00
64	2.44×10^{-3}	1.76	1.78×10^{-3}	2.00	1.51×10^{-1}	1.01
128	7.61×10^{-4}	1.68	4.46×10^{-4}	2.00	7.55×10^{-2}	1.00
256	3.04×10^{-4}	1.33	1.11×10^{-4}	2.00	3.77×10^{-2}	1.00
512	1.32×10^{-5}	1.20	2.79×10^{-5}	2.00	1.89×10^{-2}	1.00

comparison, we also include the numerical results of Galerkin bilinear IFEM solutions without partial penalty in Table 3. Convergence in the L^∞ norm is not optimal.

Next we consider a larger coefficient jump, i.e., $(\beta_1, \beta_2, \beta_3) = (100, 10000, 1)$. The errors of PPIFEM and Galerkin IFEM are reported in Tables 4 and 5, respectively. It can be observed that the PPIFEM scheme is robust for this large contrast case in all three norms. Again, the convergence of L^∞ norm for Galerkin IFEM is suboptimal. The magnitudes of the errors are significant larger than the errors of PPIFEM solutions.

Table 4
PPIFEM errors in Example 1 with coefficients $(100, 10000, 1)$.

N	$\|u_h - u\|_{L^\infty}$	Order	$\|u_h - u\|_{L^2}$	Order	$|u_h - u|_{H^1}$	Order
16	8.87×10^{-3}		2.81×10^{-2}		6.44×10^{-1}	
32	2.93×10^{-3}	1.60	7.10×10^{-3}	1.98	3.25×10^{-1}	0.99
64	7.30×10^{-4}	2.00	1.78×10^{-3}	2.00	1.63×10^{-1}	1.00
128	1.81×10^{-4}	2.01	4.45×10^{-4}	2.00	8.16×10^{-2}	1.00
256	4.43×10^{-5}	2.04	1.11×10^{-4}	2.00	4.08×10^{-2}	1.00
512	1.16×10^{-5}	1.93	2.78×10^{-5}	2.00	2.04×10^{-2}	1.00

Table 5
IFEM errors in Example 1 with coefficients $(100, 10000, 1)$.

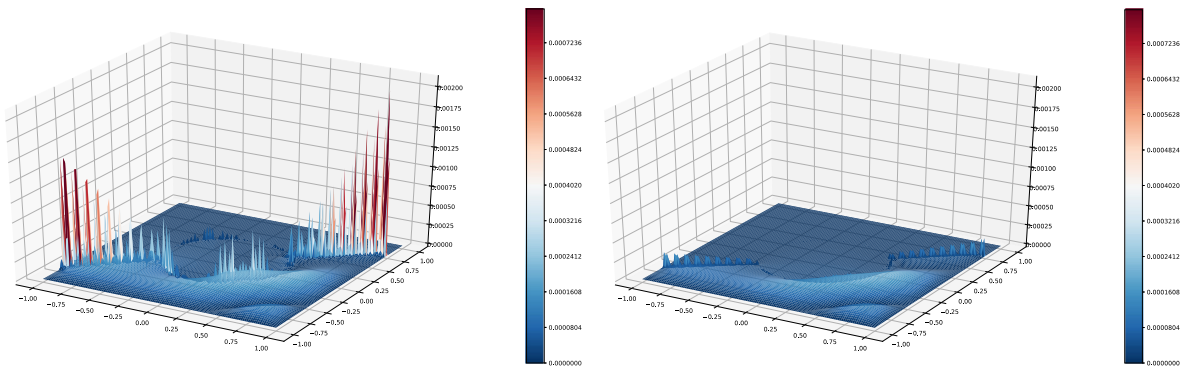| N	$\|u_h - u\|_{L^\infty}$	Order	$\|u_h - u\|_{L^2}$	Order	$|u_h - u|_{H^1}$	Order
16	9.27×10^{-3}		2.80×10^{-2}		6.43×10^{-1}	
32	2.84×10^{-3}	1.71	7.10×10^{-3}	1.98	3.25×10^{-1}	0.98
64	8.51×10^{-4}	1.74	1.78×10^{-3}	2.00	1.63×10^{-1}	1.00
128	4.54×10^{-4}	0.91	4.45×10^{-4}	2.00	8.16×10^{-2}	1.00
256	2.35×10^{-4}	0.95	1.11×10^{-4}	2.00	4.08×10^{-2}	1.00
512	1.19×10^{-4}	0.98	2.79×10^{-5}	2.00	2.04×10^{-2}	1.00

Fig. 8. Comparison of error surfaces of classical IFEM and PPIFEM for Example 2.

5.2. Example 2

In this example, we test our numerical scheme for curved interfaces. In particular, the interfaces consist of a circle and a straight line, which are defined by the following level set functions

$$\varphi_1(x, y) = 3x - 4y,$$
$$\varphi_2(x, y) = x^2 + y^2 - 0.25,$$
$$\varphi_3(x, y) = -x^2 - y^2 + 0.25.$$

The exact solution is set to be

$$u_1(x, y) = \frac{1}{\beta_1}((x^2 + y^2)^{1.5} - 0.125),$$
$$u_2(x, y) = \frac{1}{\beta_2}(x^2 + y^2 - 0.25)\sin(3x - 4y),$$
$$u_3(x, y) = \frac{1}{\beta_3}(3x - 4y)\ln(x^2 + y^2 + 0.75).$$

In the first case, we choose the coefficient to be $(\beta_1, \beta_2, \beta_3) = (10, 1, 100)$. The error of the interpolation operator is reported in Table 6. Errors of symmetric PPIFEM and Galerkin IFEM are reported in Tables 7 and 8, respectively. From these tables, we can see that the PPIFEM converge optimally in L^∞, L^2 and H^1 norms. The Galerkin IFE solutions have suboptimal convergence in L^∞ norm. Also, as the mesh size decreases, there seems to be an order deterioration in L^2 and H^1 norms for the Galerkin IFEM. In Fig. 8, we compare the error surfaces of classical IFEM and the PPIFEM. This clearly demonstrates that PPIFEM outperforms the classical IFEM in terms of the accuracy around the interface.

We also consider a large coefficient contrast case, $(\beta_1, \beta_2, \beta_3) = (100000, 100, 10)$. The errors of symmetric PPIFEM and Galerkin IFEM are reported in Tables 9 and 10, respectively. The convergences are similar to above.

Table 6
Interpolation errors and convergences of Example 2 with coefficients $(10, 1, 100)$.

N	$\|\mathcal{I}_h u - u\|_{L^2}$	Order	$|\mathcal{I}_h u - u|_{H^1}$	Order
16	2.46×10^{-2}		5.27×10^{-1}	
32	6.25×10^{-3}	1.98	2.63×10^{-1}	1.00
64	1.57×10^{-3}	1.99	1.31×10^{-1}	1.00
128	3.93×10^{-4}	2.00	6.57×10^{-2}	1.00
256	9.84×10^{-5}	2.00	3.28×10^{-2}	1.00
512	2.46×10^{-5}	2.00	1.64×10^{-2}	1.00

Table 7
PPIFEM errors in Example 2 with coefficients $(10, 1, 100)$.

N	$\|u_h - u\|_{L^\infty}$	Order	$\|u_h - u\|_{L^2}$	Order	$|u_h - u|_{H^1}$	Order
16	1.28×10^{-2}		2.20×10^{-2}		5.26×10^{-1}	
32	3.41×10^{-3}	1.91	5.55×10^{-3}	1.99	2.63×10^{-1}	1.00
64	9.33×10^{-4}	1.87	1.39×10^{-3}	2.00	1.31×10^{-1}	1.00
128	2.43×10^{-4}	1.94	3.48×10^{-4}	2.00	6.57×10^{-2}	1.00
256	5.84×10^{-5}	2.06	8.71×10^{-5}	2.00	3.28×10^{-2}	1.00
512	1.47×10^{-5}	1.99	2.18×10^{-5}	2.00	1.64×10^{-2}	1.00

Table 8
IFEM errors in Example 2 with coefficients $(10, 1, 100)$.

N	$\|u_h - u\|_{L^\infty}$	Order	$\|u_h - u\|_{L^2}$	Order	$|u_h - u|_{H^1}$	Order
16	4.75×10^{-2}		2.38×10^{-2}		5.42×10^{-1}	
32	1.49×10^{-2}	1.67	5.78×10^{-3}	2.04	2.68×10^{-1}	1.01
64	4.82×10^{-3}	1.63	1.43×10^{-3}	2.02	1.34×10^{-1}	1.01
128	2.09×10^{-3}	1.21	3.56×10^{-4}	2.01	6.70×10^{-2}	1.00
256	9.64×10^{-4}	1.11	9.04×10^{-5}	1.98	3.39×10^{-2}	0.98
512	4.74×10^{-4}	1.02	2.47×10^{-5}	1.87	1.75×10^{-2}	0.96

Table 9
PPIFEM errors in Example 2 with coefficients $(1000000, 100, 10)$.

N	$\|u_h - u\|_{L^\infty}$	Order	$\|u_h - u\|_{L^2}$	Order	$|u_h - u|_{H^1}$	Order
16	1.42×10^{-2}		3.29×10^{-3}		5.77×10^{-2}	
32	3.42×10^{-3}	2.05	7.22×10^{-4}	2.19	2.79×10^{-2}	1.05
64	1.32×10^{-3}	1.38	2.11×10^{-4}	1.78	1.34×10^{-2}	1.06
128	3.06×10^{-4}	2.11	3.60×10^{-5}	2.55	6.03×10^{-3}	1.15
256	1.05×10^{-4}	1.54	8.60×10^{-6}	2.07	2.92×10^{-3}	1.04
512	2.66×10^{-5}	1.98	2.07×10^{-6}	2.06	1.43×10^{-3}	1.03

Table 10
IFEM errors in Example 2 with coefficients $(1000000, 100, 10)$.

N	$\|u_h - u\|_{L^\infty}$	Order	$\|u_h - u\|_{L^2}$	Order	$|u_h - u|_{H^1}$	Order
16	2.84×10^{-3}		2.07×10^{-3}		4.59×10^{-2}	
32	2.37×10^{-3}	0.26	5.66×10^{-4}	1.87	2.40×10^{-2}	0.93
64	1.17×10^{-3}	1.02	1.85×10^{-4}	1.61	1.28×10^{-2}	0.91
128	4.60×10^{-4}	1.34	3.77×10^{-5}	2.30	6.23×10^{-3}	1.03
256	2.40×10^{-4}	0.94	1.02×10^{-5}	1.88	3.28×10^{-3}	0.93
512	1.23×10^{-4}	0.97	3.15×10^{-6}	1.70	1.82×10^{-3}	0.85

6. Conclusion

We have developed a partially penalized immersed finite element method using bilinear polynomials for solving elliptic multi-domain interface problems with triple junction points. The immersed finite element basis functions are constructed on interface elements with for all types of geometrical configurations. The local bilinear IFE spaces are enriched for handling nonhomogeneous flux jump conditions. Numerical results are provided to demonstrate the effectiveness of our method. In the future, we plan to carry on the a priori error estimates for the method and will also plan to extend the method to other interface problems.

Declaration of competing interest

The authors declare that they have no known competing financial interests or personal relationships that could have appeared to influence the work reported in this paper.

CRediT authorship contribution statement

Yuan Chen: Writing - original draft. **Songming Hou:** Conceptualization, Writing - review & editing. **Xu Zhang:** Methodology, Writing - review & editing.

References

[1] Chen Z, Zou J. Finite element methods and their convergence for elliptic and parabolic interface problems. Numer Math 1998;79(2):175–202.
[2] Peskin CS. Numerical analysis of blood flow in the heart. J Comput Phys 1977;25(3):220–52.
[3] Leveque RJ, Li Z. The immersed interface method for elliptic equations with discontinuous coefficients and singular sources. SIAM J Numer Anal 1994;31(4):1019–44.
[4] Yu S, Zhou Y, Wei G-W. Matched interface and boundary (mib) method for elliptic problems with sharp-edged interfaces. J Comput Phys 2007;224(2):729–56.
[5] Ingram DM, Causon DM, Mingham CG. Developments in Cartesian cut cell methods. Math Comput Simulation 2003;61(3–6):561–72.
[6] Babuška I. The finite element method for elliptic equations with discontinuous coefficients. Computing 1970;5:207–13.
[7] Babuška I, Banerjee U. Stable generalized finite element method (SGFEM). Comput Methods Appl Mech Engrg 2012;201:91–111.
[8] Fries T-P, Belytschko T. The extended/generalized finite element method: an overview of the method and its applications. Internat J Numer Methods Engrg 2010;84(3):253–304.
[9] Burman E, Claus S, Hansbo P, Larson M, Massing A. CutFEM: discretizing geometry and partial differential equations. Internat J Numer Methods Engrg 2015;104(7):472–501.
[10] Li Z. The immersed interface method using a finite element formulation. Appl Numer Math 1998;27(3):253–67.
[11] Li Z, Lin T, Wu X. New cartesian grid methods for interface problems using the finite element formulation. Numer Math 2003;96(1):61–98.
[12] Li Z, Lin T, Lin Y, Rogers RC. An immersed finite element space and its approximation capability. Numer Methods Partial Differential Equations 2004;20(3):338–67.
[13] He X, Lin T, Lin Y. Approximation capability of a bilinear immersed finite element space. Numer Methods Partial Differential Equations 2008;24(5):1265–300.
[14] Cao W, Zhang X, Zhang Z. Superconvergence of immersed finite element methods for interface problems. Adv Comput Math 2017;43(4):795–821.
[15] Lin T, Sheen D, Zhang X. A nonconforming immersed finite element method for elliptic interface problems. J Sci Comput 2019;79(1):442–63.
[16] Lin T, Lin Y, Zhang X. Partially penalized immersed finite element methods for elliptic interface problems. SIAM J Numer Anal 2015;53(2):1121–44.
[17] Guo R, Lin T, Zhuang Q. Improved error estimation for the partially penalized immersed finite element methods for elliptic interface problems. Int J Numer Anal Model 2019;16(4):575–89.
[18] Ji H, Zhang Q, Wang Q, Xie Y. A partially penalised immersed finite element method for elliptic interface problems with non-homogeneous jump conditions. East Asia J Appl Math 2018;8(1):1–23.
[19] Guo H, Yang X, Zhang Z. Superconvergence of partially penalized immersed finite element methods. IMA J Numer Anal 2017;38(4):2123–44.
[20] Xia K, Zhan M, Wei G. MIB method for elliptic equations with multi-material interfaces. J Comput Phys 2011;230(12):4588–615.
[21] Hou S, Wang L, Wang W. A numerical method for solving the elliptic interface problems with multi-domains and triple junction points. J Comput Math 2012;30(5):504–16.
[22] Hou S, Wang W, Wang L. Numerical method for solving matrix coefficient elliptic equation with sharp-edged interfaces. J Comput Phys 2010;229(19):7162–79.
[23] Wang L, Hou S, Shi L. A numerical method for solving three-dimensional elliptic interface problems with triple junction points. Adv Comput Math 2018;44(1):175–93.
[24] Wang L, Hou S, Shi L, Solow J. A numerical method for solving elasticity equations with interface involving multi-domains and triple junction points. Appl Math Comput 2015;251:615–25.
[25] Chen Y, Hou S, Zhang X. An immersed finite element method for elliptic interface problems with multi-domain and triple junction points. Adv Appl Math Mech 2019;11(5):1005–21.
[26] He X, Lin T, Lin Y. Immersed finite element methods for elliptic interface problems with non-homogeneous jump conditions. Int J Numer Anal Model 2011;8(2):284–301.
[27] Bramble JH, King JT. A finite element method for interface problems in domains with smooth boundaries and interfaces. Adv Comput Math 1996;6(2):109–38.
[28] Lin T, Lin Y, Rogers R, Ryan ML. A rectangular immersed finite element space for interface problems. Adv Comput: Theory Pract 2001;7:107–14.
[29] He X, Lin T, Lin Y. Approximation capability of a bilinear immersed finite element space. Numer Methods Partial Differential Equations 2008;24(5):1265–300.